lubricants

Article

A Fractal Prediction Method for Contact Stiffness of Helical Gear Considering Asperity Lateral Contact and Interaction

Xiangyang Xu [1,2,*], Lei Shi [1] and Linfang Fan [2]

[1] School of Mechatronics and Vehicle Engineering, Chongqing Jiaotong University, Chongqing 400074, China; 15696417881@163.com
[2] School of Traffic and Transportation, Chongqing Jiaotong University, Chongqing 400074, China; fanlinfang1998@163.com
* Correspondence: xuxa@cqjtu.edu.cn

Abstract: The normal contact stiffness (NCS) on rough surfaces has a significant impact on the dynamic characteristics of helical gear. Aiming at the problem of inaccurate calculation of the NCS model under the traditional Hertz theory of smooth surfaces, a fractal prediction model of helical gear contact stiffness considering asperity lateral contact and interaction between asperities is proposed in this paper. The variation formula of asperity and the correction coefficient of a tooth contact surface under asperity lateral contact and interaction are derived, and the influence of micro-elements on normal load and NCS is qualitatively analyzed. The results show that the NCS of considering the interaction and lateral contact of asperity is closer to the experimental results; the contact surface correction coefficient increases with the increase of curvature radius and load. The NCS of a tooth surface increases with the increase in fractal dimension D or the decrease in roughness amplitude G. The influence of asperity lateral contact and interaction decreases with the increase in D and the decrease in G. The NCS of the helical gear decreases under the lateral contact and interaction of the asperity, which is critical for exact estimation of the NCS of contact surfaces in gear.

Keywords: normal contact stiffness; helical gear; fractal theory; asperity lateral contact

check for updates

Citation: Xu, X.; Shi, L.; Fan, L. A Fractal Prediction Method for Contact Stiffness of Helical Gear Considering Asperity Lateral Contact and Interaction. *Lubricants* **2023**, *11*, 509. https://doi.org/10.3390/lubricants11120509

Received: 13 October 2023
Revised: 18 November 2023
Accepted: 27 November 2023
Published: 30 November 2023

1. Introduction

Normal contact stiffness (NCS) is a key factor affecting dynamic contact performance and load-carrying properties of helical gear, which is usually calculated using the Hertz contact theory [1]. However, Hertz theory ignores the influence of rough surface microscopic parameters on gear contact, which will affect the strength calculation of gear and the selection of design parameters. Therefore, it is important to study the effect of the rough surface micro-morphology on NCS, which is helpful for promoting the performance of helical gear.

Many scholars have carried out research on the models that consider the effect of the micro-morphology on surface contact analysis, including the Greenwood–Williamson (G-W) model, the Kogut–Etsion (K-E) model, and the fractal model [2–4]. Because the fractal model is not limited by the instrument resolution and sampling length, the fractal theory is used to study the NCS of helical gear. Liu et al. [5] established a model of the NCS of the micro-segment gear considering the influence of friction factors by referring to the fractal theory. Huang et al. [6] described the transmission error of the high-contact-ratio spur gear based on fractal theory, calculated the time-varying mesh stiffness of the gear, and analyzed the effect of the micro-morphology of the tooth surface on the dynamic response. Wang et al. [7] established the fractal contact model of the cylinder loading-unloading process with friction. Wang et al. [8] analyzed the NCS of micro-pitting gear by simulating the fractal parameters of micro-pitting, and revealing the affection of gear surface micro-parameters on NCS. Wang et al. [9] established the fractal model of NCS of mechanical joints, which takes into account the interaction of asperity, and analyzed the effect of the interaction of asperity.

Microscopically, the real machined surface is much rougher, and it is covered by innumerable asperities. When two rough surfaces contact each other, there are mainly lateral contacts between the upper and lower asperities in the interface [10]. Therefore, Zhou et al. [10] discussed the micro-contact characteristics of gears, considering the affection of lateral contact of asperity. Chen et al. [11] simulated the contact of asperity and explored the effect of the asperity lateral contact on the overall contact. Zhang et al. [12] explored the NCS of the contact surface based on the fractal theory, considering the lateral contact of asperity. However, given the closer distance between neighboring asperities for a higher load or a larger ratio of real contact to nominal area, the assumption of isolated asperity contact without any interaction is not realistic.

On the basis of the above research theories and applications of the fractal model of contact surface, the variation mechanism of the asperity under the combined influence of the asperity lateral contact and interaction is considered in the present paper. Combining with the meshing process of the helical gear pair, the contact surface correction coefficient of the helical gear was constructed, and the accurate fractal prediction model of the NCS of the helical gear was derived. Then, the characteristics of the tooth surface contact bearing capacity and NCS were further studied. Furthermore, the effects of surface morphology on NCS are discussed.

2. The Fractal Contact Mechanism under Asperity Lateral Contact and Interaction

The micro-contact behavior on the contact surface of the helical tooth was analyzed to gain the deformation of the asperity under the combined affection of the lateral contact and the interaction of the asperity, which paves the way for the construction of the fractal model of helical gear contact stiffness.

2.1. Characterization and Reconstruction of Rough Gear Surface

In view of the fractal theory, the micro-morphology of the gear surface was characterized and reconstructed [13]. The two-dimensional fractal surface morphology is mainly described by the Weierstrass–Mandelbrot (W-M) function [14].

$$z(x) = G^{(D-1)} \sum_{n=n_{min}}^{\infty} \frac{\cos 2\pi\gamma^n x}{\gamma^{(2-D)n}} \tag{1}$$

where $z(x)$ denotes the random height of the rough surface profile; x denotes the displacement coordinate of the corresponding $z(x)$; and D is the fractal dimension, which represents the irregularity and complexity of the fractal surface. In general, a larger fractal dimension D denotes a smoother contact surface, where the micro-profile of the rough surface is more sophisticated, with a deeper self-similarity; G is the roughness amplitude, which characterizes the magnitude of the surface profile, indicating the flatness in the vertical direction of the contact surfaces; γ_n denotes the spatial frequency of the rough surface profile; and n denotes the frequency index of the asperity.

Figure 1 shows the micro-topography of the gear surface. The profile parameter $z(x)$ can be processed using the structural function method, and the corresponding D and G can be measured. The specific calculation method and the corresponding 3D fractal surface morphology function can be found in Ref. [15].

According to the characterization parameters D and G measured using the experiments shown in Figure 1, the micro-topography of the gear surface could be reconstructed, as shown in Figure 2. It can be observed that the micro-topography of the gear surface was well simulated by fractals.

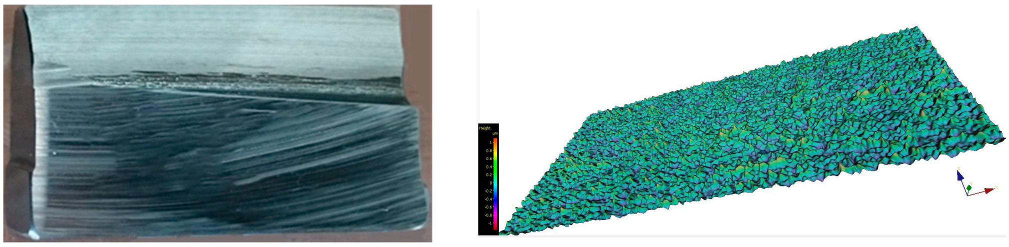

(**a**) (**b**)

Figure 1. Measurement of gear surface micro-topography: (**a**) specimen, (**b**) 3D micro-topography of gear surface.

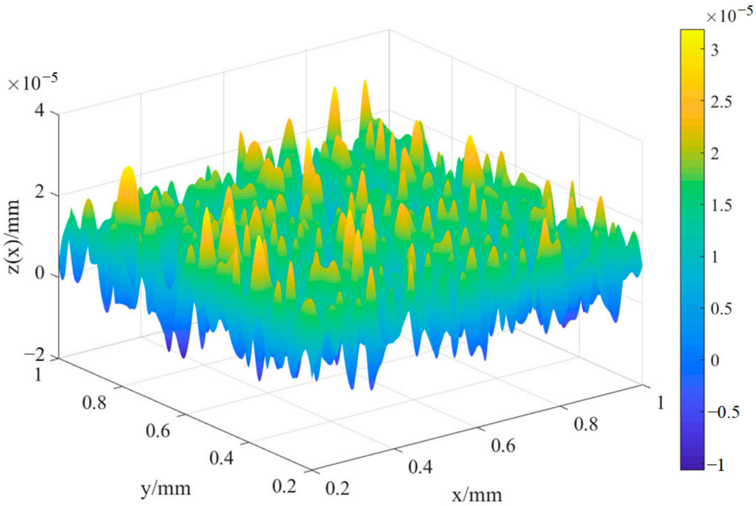

Figure 2. Reconstruction of 3D fractal rough surface.

2.2. Analysis of Asperity Lateral Contact and Interaction

The fractal contact model assumes that when the rough surfaces contact, the contact between asperities is the contact between the rough peak and the rough peak, but in the actual contact process, the asperities are mostly shoulder-to-shoulder contact, also known as lateral contact [12].

2.2.1. Analysis of Lateral Contact of Asperities

To facilitate the construction of a mathematical model of the lateral contact of the asperities, this study only focused on normal elastic–plastic behavior under non-adhesive conditions, neglecting interface shear strength and tangential friction.

As shown in Figure 3, a pair of laterally contacted asperities were selected. The contact angle between asperities is represented by α; p_a is the contact load; and p_t and p_n are the horizontal and vertical components of p_a, respectively. The following expressions are known from the geometric relation of graphs: $\cos\alpha = \left(1 + r_a^2/R_s^2\right)^{-1/2}$, $p_n = p_a \cos\alpha$, $R(y) = R\left(1 + r_a^2/R_s^2\right)^{3/2}$ [16]. The relationship between the asperity lateral contact deformation δ_a and the asperity positive contact deformation δ_p is:

$$\delta_a = \left(\delta_p - \frac{r_a^2}{2R_s}\right)\left(1 + \frac{r_a^2}{R_s^2}\right)^{-\frac{1}{2}} \tag{2}$$

where r_a is the tangential offset of the contact asperities; R is the equivalent curvature radius of the vertices of the asperities; $R(y)$ is the equivalent curvature radius of the contact points of the two asperities; y is the offset between the intersection midpoint of the asperity and the peak value of the rough surface; and R_s is the sum of the asperity radii R_1 and R_2. It is known that $R = a^{D/2}G^{1-D}/\pi^2$ [17], based on the above geometric relationship of the lateral contact of the asperities, the relationship between the contact area a_a in the lateral contact and the contact area a_p in the positive contact of the asperities can be obtained as follows:

$$a_a = a_p \left(1 + \frac{r_a^2}{R^2}\right)^{\frac{3}{D}} \tag{3}$$

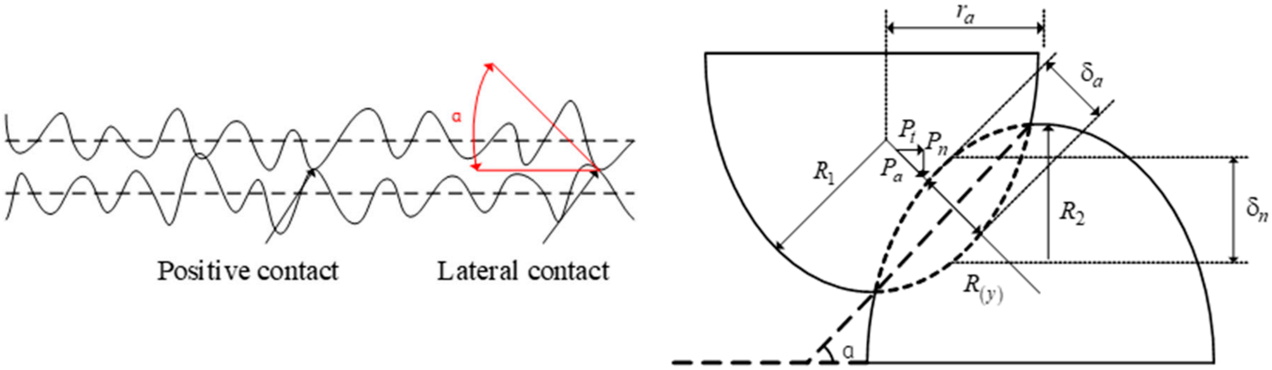

(**a**) (**b**)

Figure 3. Asperity contact diagram: (**a**) contact between rough surfaces, (**b**) lateral contact of asperity.

2.2.2. Force Analysis of Asperity Interaction

Figure 4 shows the contact situation of two rough surfaces and the contact situation of the asperity. Considering the effect of asperity interaction, the total deformation is $\delta_1 = \delta_p - \delta'$ [17]. Specifically, it is expressed as $\delta_1 = \left(9F^2/16E^2R\right)^{1/3}$. It can be known that the displacement of the mean plane caused by the interaction between asperities is $\delta' = p_1\sqrt{a}/(aE)$ [18]. Where F is the force exerted on the rough peak; E denotes the composite Young's modulus of the contact material. In Figure 4, Z is the profile height data of a given asperity, with the average plane as the measurement benchmark; d is the distance between the rigid smooth surface and the average of the original roughness; d_n is the distance between the rigid smooth surface and the average plane of asperity after the normal load deformation of the joint surface [17].

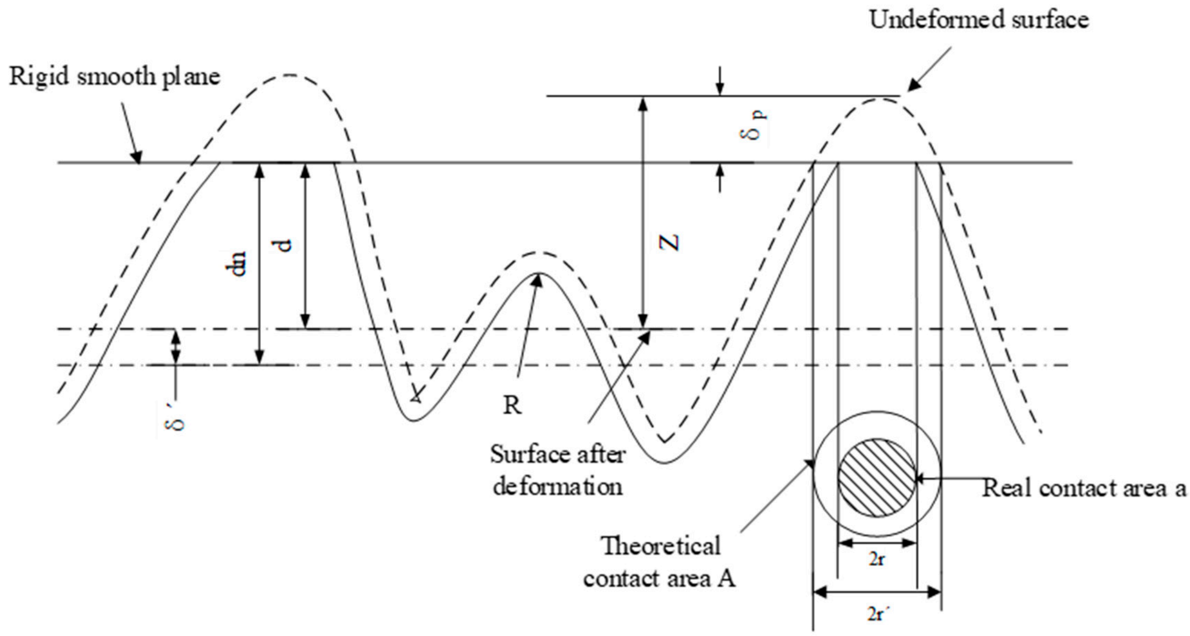

Figure 4. Contact equivalent interface between rough surfaces.

Moreover, Wang's model equates the contact between rough surfaces to asperity positive contact without considering that asperity is basically lateral contact when the rough surfaces are contacted [9]. Considering the common influence of asperity lateral contact and interaction, the deformation of asperity in the direction of a is obtained as follows:

$$\delta_a = \left(\left(\frac{9p^2}{16E^2R} \right)^{\frac{1}{3}} - \frac{r_a^2}{2R_s} \right) \left(1 + \frac{r_a^2}{R_s^2} \right)^{-\frac{1}{2}} \tag{4}$$

2.2.3. Contact Deformation Analysis of Helical Gear Surface

The contact between the helical gear surface is point contact. When the load is applied, the contact point expands instantaneously into an ellipse. When point contact is extended to elliptical contact, the stress distribution on the contact surface of the ellipse $p(x, y)$ is shown in Figure 5.

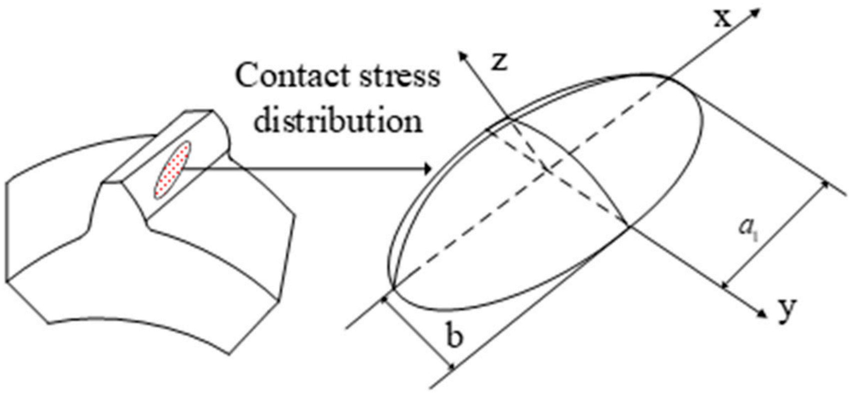

Figure 5. Distribution of contact stress of helical gear.

The contact deformation in the contact area of the ellipse is [19]: $\varepsilon(x, y) = (3a_1 b p_m / 4E) \int_0^\infty (1 - (x^2/a_1{}^2 + \omega) - (y^2/b^2 + \omega))d\omega / \sqrt{(a_1{}^2 + \omega)(b^2 + \omega)\omega}$, where $\left(x^2/a_1{}^2 + \omega\right) + \left(y^2/b^2 + \omega\right) = 1$; a_1 is the long axis of the contact ellipse; b is the short axis of the contact ellipse; and p_m is the average contact pressure.

In summary, the total deformation $\delta_a(x, y)$ of the asperity in direction a, can be obtained from the following equation:

$$\delta_a(x, y) = \left(\left(\frac{9p^2}{16E^2R} \right)^{\frac{1}{3}} - \frac{r_a^2}{2R_s} - \varepsilon(x, y) \right) \left(1 + \frac{r_a^2}{R_s^2} \right)^{-\frac{1}{2}} \tag{5}$$

3. The Fractal Model of NCS of Helical Gear

In practical industrial applications, components such as gears and rolling bearings in mechanical systems typically work in mixed-lubrication contact [20]. As shown in Figure 6, for helical gear under mixture lubrication, since the load is borne by the asperity and lubricating oil, the NCS of the helical tooth is mainly composed of the NCS of the asperity part and the oil film part. The mean plane of the fractal surface is taken as the reference plane for the lubricant contact. When the NCS (K) is calculated, it is equivalent to the parallel model of the NCS of the solid part (K_s) and the NCS of the oil film part (K_l) according to the load distribution idea. Then, the equivalent comprehensive NCS is $K_s + K_l$.

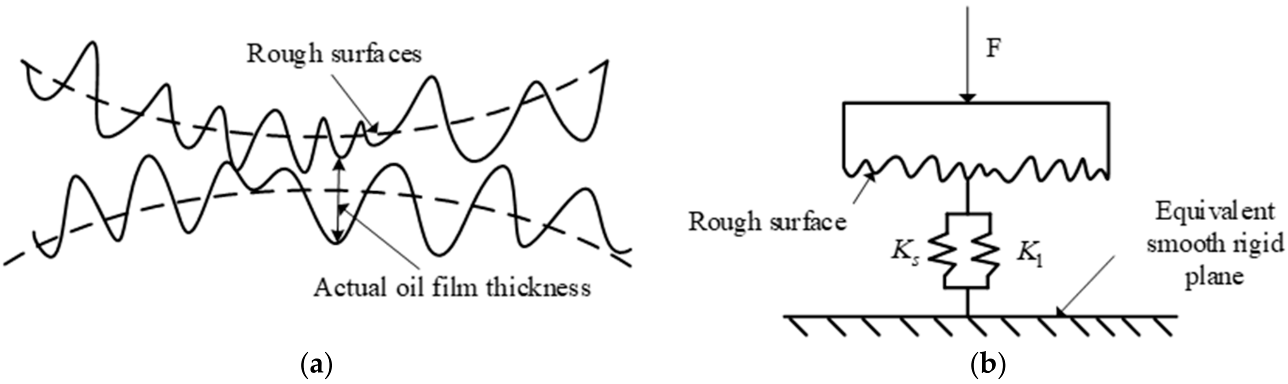

Figure 6. Contact diagram of joint surface under mixed lubrication: (**a**) equivalent interface, (**b**) parallel contact mode.

3.1. Relationship between Contact Load and Contact Area of Single Asperity

In the elastic deformation stage, the contact area a is expressed as [5]: $a = \pi R\delta$. When the deformation of asperity is $\delta_a(x, y)$, the contact area a_{ae} in the elastic deformation stage of asperity is:

$$a_{ae} = \pi R\delta_a \left(1 + \frac{r_a^2}{R^2}\right)^{\frac{3}{2}} \tag{6}$$

According to Equation (3), the contact load of a single asperity is $F_{ae} = 4\sqrt{\pi}EG^{D-1} a^{(3-D)/2}\left(1 + r_a^2/R^2\right)^{(9-3D/2D)}/3$. The contact pressure of asperity is specifically expressed as:

$$\Delta P_{ae}(a) = \frac{4EG^{D-1}a^{\frac{3-D}{2}}}{3\sqrt{\pi}R}\left(\left(\frac{9p^2}{16E^2R}\right)^{\frac{1}{3}} - \frac{r_a^2}{2R_s} - \varepsilon(x, y)\right)^{-1}\left(1 + \frac{r_a^2}{R^2}\right)^{\frac{9-6D}{2D}} \tag{7}$$

Friction has a significant impact on gear contact performance [21]; when considering the friction, the asperity will begin to yield at the critical average pressure $P_\mu = 1.1k_\mu Y$, where k_μ is the friction correction coefficient [13]. Y is the yield strength of softer materials. The critical elastic deformation area a_{aec} of asperity can be obtained by Equation (10).

$$a_{aec} = \left(\frac{16E^2G^{2D-2}\left(1+\frac{r_a^2}{R^2}\right)^{\frac{9-6D}{D}}}{3.3^2\pi k_\mu{}^2Y^2R^2\delta_a{}^2}\right)^{\frac{1}{D-3}} \tag{8}$$

Therefore, in the elastic deformation stage of the asperity, the contact load F_{ae} is as follows:

$$F_{ae} = \tfrac{2}{3}KHa_{aec}{}^{0.5}a^{0.5}\left(1 + \tfrac{r_a^2}{R^2}\right)^{\frac{3}{2D}} \tag{9}$$

When the deformation of asperity satisfies $1 \le \delta/\delta_{aec} \le 6$, the corresponding contact area is $a_{aepc} < a < a_{aec}$; the deformation is defined as the first stage of elastic-plastic deformation. At this stage, the contact load F_{aep1} is as follows:

$$F_{aep1} = 2.8KYa_{aec}^{-c_2}a^{c_2+1}\left(1 + \tfrac{r_a^2}{R^2}\right)^{\frac{3c_2+3}{D}} \tag{10}$$

When the deformation of the asperity satisfies $6 \le \delta/\delta_{aec} \le 110$, the corresponding contact area of the asperity is $a_{apc} < a < a_{aepc}$, and the deformation is defined as the second-stage elastic–plastic deformation. At this stage, the contact load F_{aep2} is as follows:

$$F_{aep2} = KBYa_{aec}^{-c_4} \cdot a^{c_4+1}\left(1+\frac{r_a^2}{R^2}\right)^{\frac{3c_4+3}{D}} \quad (11)$$

where K is the correlation coefficient between hardness H and yield strength Y; B, c_2 and c_4 are coefficients. δ_{aec} is the elastic critical deformation of asperity [22]. The elastic–plastic critical contact area $a_{aepc} = 6^{1/1-D}a_{aec}$, and the plastic critical contact area $a_{apc} = 110^{1/(1-D)}a_{aec}$ [23].

When $a < a_{apc}$, the asperity enters the complete plastic stage. The contact load F_{ap} is as follows:

$$F_{ap} = Ha\left(1+\frac{r_a^2}{R^2}\right)^{\frac{3}{D}} \quad (12)$$

3.2. The Contact Surface Correction Coefficient of Helical Gear

In fractal theory, the area distribution function $n(a)$ proposed by Majumdar and Bhushan is modified to establish a functional relationship between contact area and load, thereby studying the trend of changes in the influence of different parameters on contact load. However, the area distribution function is only applicable to the mechanical joint plane, which is not applicable to the contact between gear rough surfaces. Therefore, a correction coefficient λ_C is constructed to correct the area distribution function $n(a)$. If two helical gears are of the same material and isotropic, the adjusted $n(a)'$ is expressed as follows when the two gears are in contact:

$$n(a)' = \lambda_C \frac{D}{2} a_l^{\frac{D}{2}} a^{-\frac{D+2}{2}} \quad (13)$$

where a_l is the maximum contact area of a single asperity on the contact surface, and the specific form of λ_C is $\lambda_c = (S/\sum S)^{X_h}$ [24]. S is the contact area of the gear; $\sum S$ is the sum of the surface area of two contact bodies; and X_h is the total curvature factor of the gear teeth.

$S = \pi a_1 b$, where the long axis a_1 and the short axis b of the contact ellipse, the specific expression references [25], and S can be expressed as:

$$S = \sqrt{\frac{\pi F L d_1 d_2 \cos\alpha_t \tan\alpha_t'}{2E(d_1+d_2)\cos\beta_b}} \quad (14)$$

The long axis of the ellipsoid is $A_j = \sqrt{r_{jx}^2 - \left(r_{jx} - r_{jy}\right)^2}$; the short axis is $B_j = r_{jy}$ [19]; r_{jx} and r_{jy} are the principal curvature radii of the two ellipsoids; $j = 1, 2$ means the contact between the two ellipsoids of the driving and driven gears; and $\sum S$ can be obtained as:

$$\sum S = \frac{8\pi}{3}\sum_{j=1}^{2}\left(A_j B_j\right) \quad (15)$$

The comprehensive curvature radius at the contact point is [25] $\rho = d_1 d_2 \cos\alpha_t \tan\alpha_t' / (2(d_1+d_2)\cos\beta_b)$. R_1 and R_2 are the node normal curvature radii of the driving gear and driven gear, respectively; d_1 and d_2 are the diameters of the gear pitch circle; α_t is the transverse pressure angle; α_t' is the meshing angle; and β_b is the spiral angle of the base circle. The comprehensive curvature coefficient $X_h = 1/\rho$. According to the above, it can be known that the contact surface correction coefficient λ_C is:

$$\lambda_C = \left(\frac{3S_1+3S_2}{8\pi(A_1B_1+A_2B_2)}\right)^{\frac{2(d_1+d_2)\cos\beta_b}{d_1 d_2 \cos\alpha_t \tan\alpha_t'}} \quad (16)$$

3.3. Establishment of Fractal Model for NCS of Helical Gear

The normal stiffness of the asperity, which is elastically deformed, can be deduced from the derivative of the elastic contact load to the surface interference, the NCS of a single asperity in the elastic stage, as follows:

$$k_{sae} = \frac{2\pi KHR{a_{aec}}^{0.5}}{3a^{0.5}}\left(1+\frac{r_a^2}{R^2}\right)^{\frac{3D-3}{2D}} \tag{17}$$

The NCS of a single asperity in the first elastic–plastic stage and the NCS in the second elastic–plastic stage are as follows:

$$\begin{cases} k_{saep1} = 2.8\pi KYRa_{aec}^{-c_2}a^{c_2}\left(1+\frac{r_a^2}{R^2}\right)^{\frac{12c_2+3D+6}{2D}} \\ k_{saep2} = \pi KBYRa_{aec}^{-c_4}\cdot a^{c_4}\left(1+\frac{r_a^2}{R^2}\right)^{\frac{12c_4+3D+6}{2D}} \end{cases} \tag{18}$$

Due to the influence of the asperity lateral and interaction, the curvature radius, the offset, and the contact angle α_i of the contact point are different. It is supposed that when the contact angle is α_i $(\alpha_i \in [0,90])$, the total contact area of the asperity contacted at this angle in the contact area is A_i. Correspondingly, the total contact area can be expressed as $\sum_{i=1}^{imax} A_i = A_r$. According to the change of contact load on the contact surface, the rough surface will undergo three deformation stages that include the elastic deformation, the elastic–plastic deformation, and the total plastic deformation. When α_i is the contact angle, the contact area of the asperity at each stage and the total contact area on the contact surface can be expressed as follows: the elastic contact area $A_{aie} = (A_i/A_r)\int_{a_{aec}}^{a_l} n(a)'d(a)\int_{a_{aepc}}^{a_{aec}} n(a)'ad(a)$; the first stage of the elastic–plastic contact area $A_{aiep1} = (A_i/A_r)\int_{a_{aepc}}^{a_{aec}} n(a)'ad(a)$; the second stage of the elastic–plastic contact area $A_{aiep2} = (A_i/A_r)\int_{a_{apc}}^{a_{aepc}} n(a)'ad(a)$; and the full plastic contact area $(A_i/A_r)\int_0^{a_{apc}} n(a)'ad(a)$.

Then, the specific expressions are as follows:

$$\begin{cases} A_{aie} = \frac{A_i}{A_r}\frac{\lambda_C D}{2-D}{a_l}^{D/2}\left(1+\frac{r_a^2}{R^2}\right)^{3/2}\left({a_l}^{\frac{2-D}{2}}\left(1+\frac{r_a^2}{R^2}\right)^{(6-3D)/2D} - a_{aec}^{\frac{2-D}{2}}\right) \\ A_{aiep1} = \frac{A_i}{A_r}\frac{\lambda_C D}{2-D}{a_l}^{D/2}\left(1+\frac{r_a^2}{R^2}\right)^{3/2}\left(a_{aec}^{\frac{2-D}{2}} - a_{aepc}^{\frac{2-D}{2}}\right) \\ A_{aiep2} = \frac{A_i}{A_r}\frac{\lambda_C D}{2-D}{a_l}^{D/2}\left(1+\frac{r_a^2}{R^2}\right)^{3/2}\left(a_{aepc}^{\frac{2-D}{2}} - a_{apc}^{\frac{2-D}{2}}\right) \\ A_{aip} = \frac{A_i}{A_r}\frac{\lambda_C D{a_l}^{D/2}}{2-D}\left(1+\frac{r_a^2}{R^2}\right)^{3/2}(a_{apc})^{\frac{2-D}{2}} \end{cases} \tag{19}$$

For asperity with contact angle α_i at (x,y), the total contact area is expressed as:

$$A_{ri}(x,y) = \begin{cases} \frac{A_i}{A_r}(A_{aip}+A_{aiep2}+A_{aiep1}+A_{aie}) & a_l > a_{aec} \\ \frac{A_i}{A_r}(A_{aip}+A_{aiep2}+A_{aiep1}) & a_{aepc} < a_l < a_{aec} \\ \frac{A_i}{A_r}(A_{aip}+A_{aiep2}) & a_{apc} < a_l < a_{aepc} \\ \frac{A_i}{A_r}A_{aip} & a_l < a_{apc} \end{cases} \tag{20}$$

In summary, at the contact surface (x,y), the actual contact area can be expressed as:

$$A_r(x,y) = \sum_{i=1}^{i_{max}} A_{ri}(x,y) \tag{21}$$

Similarly, the elastic contact load generated by the asperity is obtained as $P_{aie} = (A_i/A_r)\int_{a_{aec}}^{a_l} F_{ae}n(a)'d(a)$. Moreover, the first stage of the elastic–plastic contact load is $P_{aiep1} = (A_i/A_r)\int_{a_{aepc}}^{a_{aec}} F_{aep1}n(a)'d(a)$; the second stage of the elastic–plastic contact load is $P_{aiep2} = (A_i/A_r)\int_{a_{apc}}^{a_{aeqc}} F_{aep2}n(a)'d(a)$; and the full plastic contact load is $P_{aip} = (A_i/A_r)\int_0^{a_{apc}} F_{ap}n(a)'d(a)$.

Due to $P_n = P_a \cos\alpha$, the normal force generated by the different contact angle α_i can be expressed as:

$$P_{ni}(x,y) = \begin{cases} \frac{A_i}{A_r}\left(P_{aip} + P_{aiep2} + P_{aiep1} + P_{aie}\right)\cos\alpha_i & a_l > a_{aec} \\ \frac{A_i}{A_r}\left(P_{aip} + P_{aiep2} + P_{aiep1}\right)\cos\alpha_i & a_{aepc} < a_l < a_{aec} \\ \frac{A_i}{A_r}\left(P_{aip} + P_{aiep2}\right)\cos\alpha_i & a_{apc} < a_l < a_{aepc} \\ \frac{A_i}{A_r}P_{aip}\cos\alpha_i & a_l < a_{apc} \end{cases} \tag{22}$$

In summary, the total normal force $P_n(x,y)$ at the contact surface (x,y) is as follows:

$$P_n(x,y) = \sum_{i=1}^{i_{max}} P_{ni}(x,y) \tag{23}$$

According to Ref. [12], the lateral contact distribution of asperity can be assumed to be Gaussian distribution and uniform distribution, where the given $1 + r_a^2/R^2$ is $\{1, 1.1, 1.2, \ldots, 1.8, 1.9\}$. For the uniform distribution, $A_i/A_r = \{0.1, 0.1, 0.1, \ldots, 0.1, 0.1\}$ can be taken. When the value of $1 + r_a^2/R^2$ is 1.1 and set to an average point, and the standard deviation is set to 0.4, for the Gaussian distribution, $A_i/A_r = \{0.2, 0.18, 0.16, 0.14, 0.1, 0.08, 0.06, 0.035, 0.025, 0.02\}$ is taken.

According to the contact stress distribution $p(x,y)$ on the contact ellipse, the uniform force at (x,y) can be obtained, and then the deformation δ' caused by the interaction of the asperities can be obtained according to Equation (4). Therefore, the total asperity deformation $\delta_a(x,y)$ and the critical elastic contact area a_{aec} are calculated. By substituting Equations (19) and (23) to get $A_r(x,y)$, $P_n(x,y)$, the relationship between the actual contact area and the total contact load of the helical gear surface, considering the lateral interaction of the asperities, is obtained as follows:

$$\begin{cases} P = \int_{-l}^{l}\int_{-b}^{b} P_n(x,y)dxdy \\ Ar = \int_{-l}^{l}\int_{-b}^{b} A_r(x,y)dxdy \end{cases} \tag{24}$$

where $l = a_1\sqrt{1 - \frac{y^2}{b}}$. Similarly, when the contact angle is α_i, the NCS is as follows:

$$\begin{aligned} k_{S\alpha_i}(x,y) &= \frac{A_i}{A_r}\left(\int_{a_{aec}}^{a_l} k_{sae}\cdot n(a)da + \int_{a_{aepc}}^{a_{aec}} k_{saep1}\cdot n(a)da + \int_{a_{apc}}^{a_{aepc}} k_{saep2}\cdot n(a)da\right) \\ &= \frac{A_i}{A_r}\frac{2\pi KHR\lambda_C(-D)}{3D+3}\left(1 + \frac{r_a^2}{R^2}\right)^{\frac{3D-3}{2D}} a_l^{D/2}a_{aec}^{0.5}\left(a_l^{\frac{-D-1}{2}} - a_{aec}^{\frac{-D-1}{2}}\right) + \\ &\frac{A_i}{A_r}\frac{5.6\pi KYR\lambda_C D}{2(2c_2-D)}\left(1 + \frac{r_a^2}{R^2}\right)^{\frac{12c_2+3D+6}{2D}} a_l^{D/2}a_{aec}^{-c_2}\left(a_{aec}^{\frac{2c_2-D}{2}} - a_{aepc}^{\frac{2c_2-D}{2}}\right) + \\ &\frac{A_i}{A_r}\frac{2\pi KBYR\lambda_C D}{2(2c_4-D)}\left(1 + \frac{r_a^2}{R^2}\right)^{\frac{12c_4+3D+6}{2D}} a_l^{D/2}a_{aec}^{-c_4}\left(a_{aepc}^{\frac{2c_4-D}{2}} - a_{apc}^{\frac{2c_4-D}{2}}\right) \end{aligned} \tag{25}$$

Figure 3 shows that $k_n = dP_n/d\delta_n = (dP_a/d\delta_a)\cos^2\alpha = K_a\cos^2\alpha$, and the total NCS of the solid part (K_s) is obtained as follows:

$$K_S = \int_{-l}^{l}\int_{-b}^{b}\sum_{i=1}^{i_{max}}\cos^2\alpha_i k_{S\alpha_i}(x,y)dxdy \tag{26}$$

According to Equation (24), the relationship between P and A_r is known. The NCS of the oil film (K_l) on the contact surface is obtained, and then the total NCS (K_n) is calculated [26] as follows:

$$K_n = \int_{-l}^{l} \int_{-b}^{b} \sum_{i=1}^{i_{max}} \cos^2 \alpha_i K_{Sai}(x, y) dxd + K_l \tag{27}$$

where the dimensionless contact load is $P^* = P/A_0E$. The dimensionless real contact area is expressed as $A_r^* = A_r/A_0$. The dimensionless NCS is expressed as $K_n^* = K_n/E\sqrt{A_0}$.

4. Influence Analysis of Fractal Contact Characteristic Parameters of Helical Gear

Based on the fractal model established in Section 3, simulation analysis was carried out. It can be seen that the dominant factors affecting the NCS of the gear included the fractal dimension, roughness amplitude, contact form of the asperity, and the oil film on the contact surface. Through the analysis, it is helpful to accurately capture the contact behavior and its change rule on the contact interface. The specific parameters of the helical gear are shown in Table 1.

Table 1. Helical gear parameters.

Parameter	Value
Number of teeth (pinion and gear)	Z_p = 33/Z_g = 28
Normal pressure angle (deg)	20
Half-face width(mm)	30
Normal module (mm)	5
Helix angle (deg)	36
Pinion torque (Nm)	1200
Pinion rotational speed (rpm)	1000
Effective elastic modulus (Pa)	2.26×10^{11}
Roughness amplitude (μm)	0.2
Asperity friction coefficient	0.12
Wear coefficient	5×10^{-4}

4.1. Model Validation

The model was validated by comparing it with other relevant prediction models and experimental data. Figure 7a shows the comparison of the NCS model of the solid part in this paper with the prediction model and experimental data in Ref. [9]. The experimental material was gray cast iron, the specific parameters are listed as follows: E = 130 GPa, HB = 231, fractal dimension D = 1.3504, $G = 2.1504 \times 10^{-12}$ m. The gear surface correction coefficient λ_C was set to 1, which is equivalent to the contact between two planes. It can be found that the change trend of the model in this paper was consistent with Wang's model [9], and the model in this paper was relatively closer to the experimental data. Although Wang considered the effect of the interaction of asperities, they were all derived under the positive contact. Wang's model only considered the elastic and plastic deformation stages of the asperity without considering the elastic–plastic deformation stage, so the larger the load, the greater the difference in NCS values between the two models. Moreover, in Wang et al.'s model, the contact between rough surfaces only considered the contact deformation of the asperity, and the load was only borne by the asperity. In the model presented in this work, the matrix was considered an elastic body, and the load was borne jointly by the asperity and the substrate. In addition, the common influence of the asperity lateral contact and interaction on the contact model can be observed in Figure 7b. It shows the comparison between the model of comprehensive NCS (K_n) in this paper and the prediction model and experimental data in Ref. [26]. The specific material parameters are listed as follows: $E = 1.3 \times 10^{11}$ Pa, $H = 8.4 \times 10^8$ Pa, in which the D = 1.342, $G = 1.11 \times 10^{-11}$ m. And the variation trend of the model in this paper was close to that of Xue's model [26] and was consistent with the change in the experimental data. This further verifies the accuracy of this model. Moreover, K_n decreased with the increase in load when the contact load was small, which can also be seen from the subsequent analysis. This is because the comprehensive equivalent NCS was dominated by the oil-film NCS.

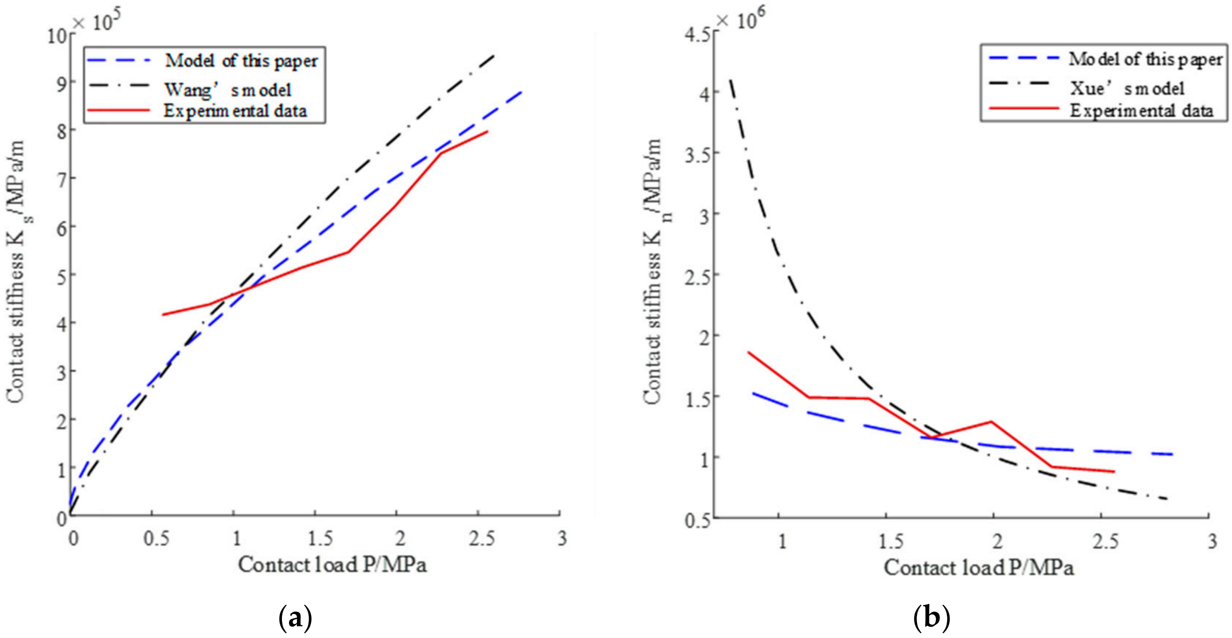

Figure 7. Model validation: (**a**) the solid part NCS, (**b**) the comprehensive NCS.

4.2. Influence of Contact Surface Correction Coefficient on Fractal Contact Characteristics of Helical Gear

According to Equation (19), the main factors influencing the correction coefficient of helical gear surface were the curvature radii R_1 and R_2, and the unit line load F. By controlling these variables, the influences of R_{12} and F on the gear surface correction coefficient λ_C were analyzed. As shown in Figure 8a, it can be found that the variation trend of λ_C with R_1 or with R_2 was roughly the same. With the increase in curvature radius, the λ_C increased, but λ_C was always less than 1. This is consistent with the setting of the correction coefficient, that is, the number of asperities in curved-surface contact is always smaller than that in plane contact. Moreover, when the radius of curvature approaches 0, the correction coefficient approaches 0, which means that there is no contact between the two rough, curved surfaces. When the radius of curvature approaches infinity, the correction coefficient approaches 1. The contact between two rough, curved surfaces is equivalent to that between two planes. In Figure 8b, when F approaches 0, λ_C is not 0, and there is no contact stress between the two contact bodies. However, due to the existence of contact entities, λ_C is not equal to 0. With the increase of load, λ_C also increases. The growth rate of λ_C gradually slows down, and λ_C is always less than 1. This is because the micro-topography makes it impossible to completely fit the two contact surfaces. Therefore, increasing the load appropriately and increasing the real contact area are conducive to improving the contact strength. The above analysis fit the classical contact theory [1], which can be verified by the rationality of the choice of λ_C.

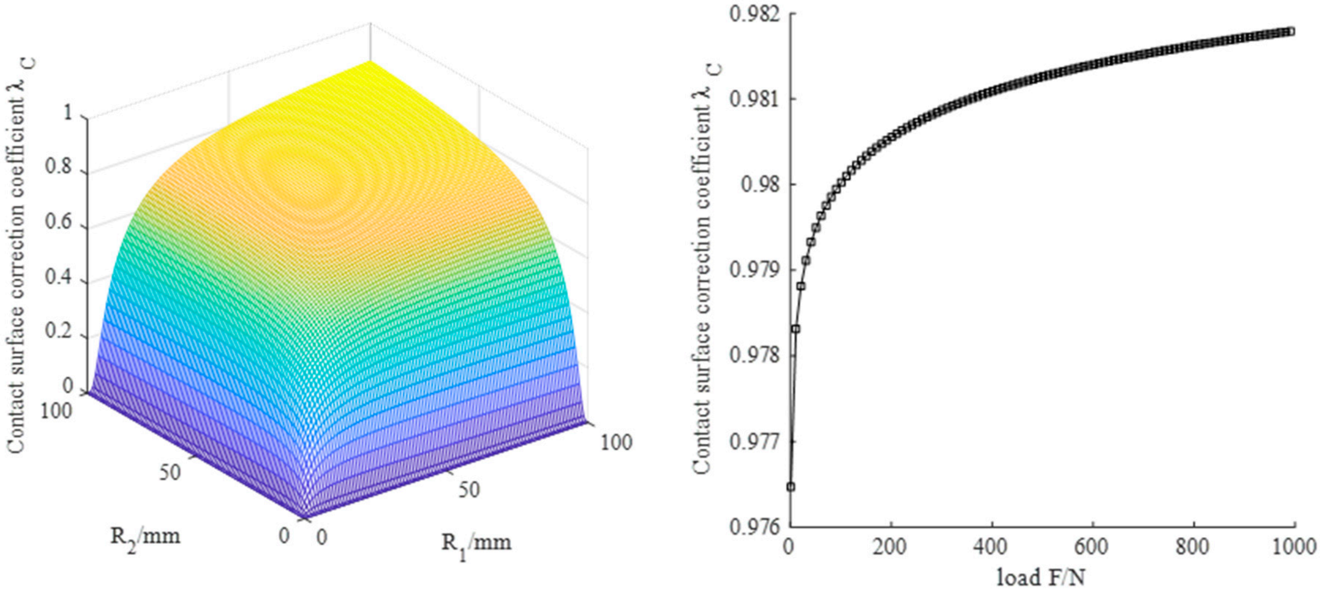

(**a**) (**b**)

Figure 8. Trend chart of contact surface correction factor: (**a**) contact surface correction factor versus curvature radius, (**b**) contact surface correction factor versus unit line load.

4.3. Effect of Fractal Dimension on Fractal Contact Characteristics of Helical Gear

The effect of fractal dimension on the contact characteristics of helical gear is shown in Figure 9, in which K_s changed with the real contact area under the influence of D and G. It can be observed from Figure 9a,b that K_s increased with the increase in the real contact area, the larger D is, the greater K_s is. This is because when G is constant, the greater the D, the smoother and more complex the contact surface is with the increase in D, and the same contact range has more scale and smaller asperities, which makes the real contact area of the contact surface larger under the same load, thereby increasing K_s of the gear surface. Similarly, Figure 9c,d shows that the relationship between K_s and A_r^* is negatively correlated with G. When the real contact area is constant, K_s decreases with the increase in G. This is because G is used as a parameter to characterize the roughness, which reflects the smoothness of the vertical direction of the contact surface. The greater the G is, the greater the amplitude of asperity is, leading to a corresponding reduction in the real contact area under the same load. It can be concluded that K_s is affected by D and G. D and G are used as parameters to characterize the rough surface to describe the surface topography. The larger D and the smaller G show that the contact surface is smoother. To summarize, reducing the roughness of the contact surface can improve the stiffness characteristics of the gear.

4.4. Effect of Oil Film on Fractal Contact Characteristics of Helical Gear

The effect of oil film on fractal contact characteristics of helical gear is shown in Figure 10a. When $D = 1.45$ and $G = 8 \times 10^{-6}$ m, K_l of the oil film changed with A_r^*. When A_r^* approached 0, K_l was the greatest. With the increase in A_r^*, K_l decreased rapidly and tended to be gentle after A_r^* was greater than 0.3, and the change was the most dramatic before A_r^* was less than 0.1. Additionally, the variation of equivalent comprehensive NCS (K_n), solid part NCS (K_s), and the oil film part NCS (K_l) with dimensionless real contact area are shown in Figure 10b. When A_r^* was small, K_s was far lower than K_l, and the equivalent comprehensive NCS was almost completely determined by K_l. Additionally, with the increase in the real contact area, the rate of K_s gradually increased, and its share in the equivalent comprehensive NCS gradually increased. The ratio of K_l to the equivalent comprehensive NCS gradually decreased, and finally it changed such that K_s dominated the equivalent comprehensive NCS. This is because when the load was small, the contact between gear surfaces was the squeeze between oil films, which is consistent with the existing research conclusions [27]. With the increase in load, the oil film was squeezed out, K_s increased sharply and K_l decreased.

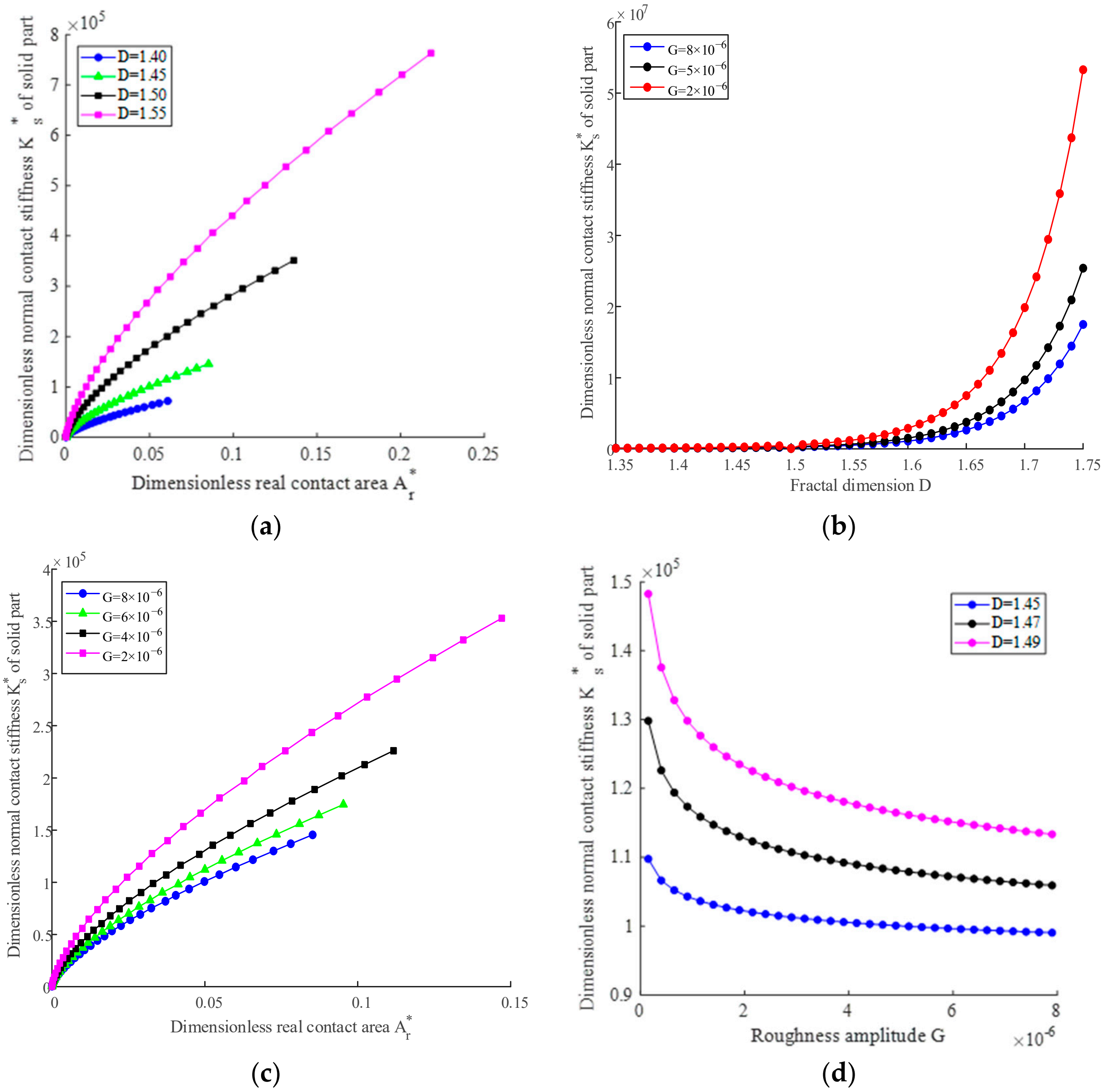

Figure 9. Effect of surface morphology on NCS of solid portion: (**a**) $G = 8 \times 10^{-6}$ m, D change, (**b**) relationship between K_s and G, (**c**) $D = 1.45$, G change, (**d**) relationship between K_s and D.

Figure 11 shows the equivalent comprehensive NCS was affected by the fractal dimension, which is similar to the change rule shown in Figure 9, but the NCS of the oil film part is considered more. It can be seen that when $A_r^* \in [0, 0.1]$, the equivalent comprehensive NCS was relatively greatly affected by the oil film. There was a minimum value when the $A_r^* > 0.1$, the NCS of the solid part, dominated. Combined with Figure 10b, it can be concluded that when the gear surface micro-topography was certain the oil film had a certain effect on the equivalent comprehensive NCS, which could effectively improve the NCS. Secondly, the micro-topography of the contact surface had a great effect on the NCS. The proportion of the real contact area to the nominal contact area can be adjusted to make the comprehensive NCS of the contact surface reach the ideal situation.

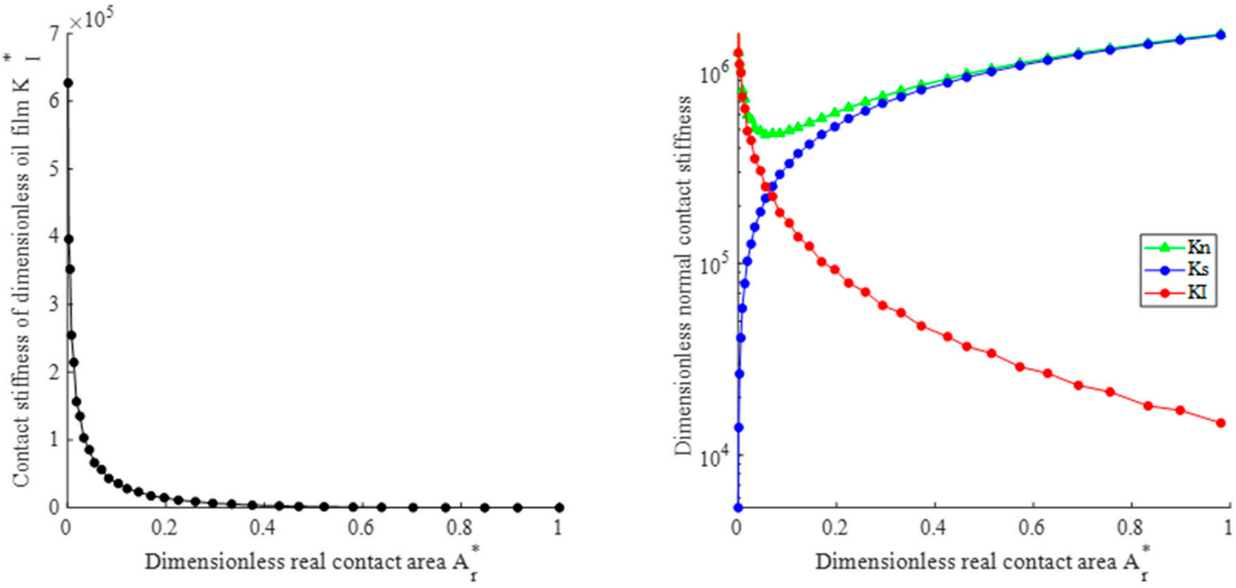

(**a**) (**b**)

Figure 10. Variation curve of NCS with contact area: (**a**) relationship between real contact area and K_l, (**b**) relationship between real contact area and NCS.

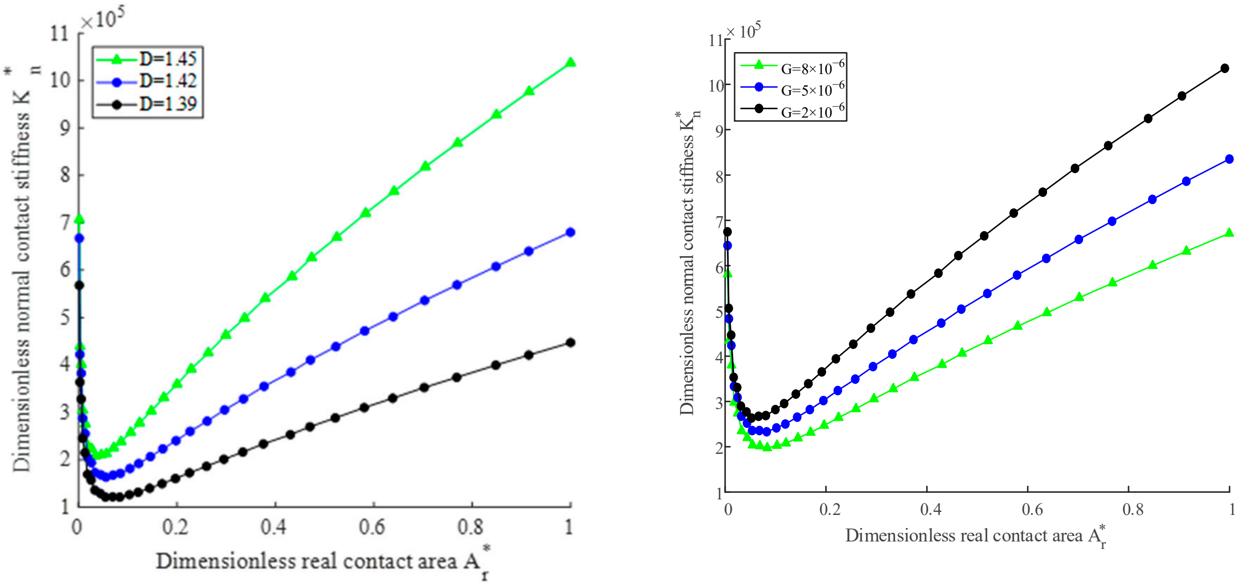

(**a**) (**b**)

Figure 11. Influence of fractal dimension on equivalent integrated NCS: (**a**) $G = 8 \times 10^{-6}$, D change, (**b**) $D = 1.40$, G change.

4.5. Effect of Asperity Lateral Contact and Interaction on Fractal Contact Characteristics of Helical Gear

The effect of asperity lateral contact and interaction on K_s is shown in Figure 12. In Figure 12a, G is 2×10^{-6} m, and D is 1.40 and 1.48, respectively. In Figure 12b, D is 1.40, and G is 8×10^{-6} m and 2×10^{-6} m, respectively. The curve with the circle represents the model without considering asperity lateral contact and interaction. The curve with the triangle represents the model with consideration of asperity lateral contact and interaction. When the load was constant, the NCS calculated by the model considering asperity lateral contact and interaction was significantly lower than that of the model without considering asperity lateral contact and interaction. This is because, when considering the lateral contact and interaction of asperity, the contact force required for the same contact deformation was greater. Therefore, when the load was constant, the contact deformation of asperity considering lateral contact and interaction was relatively small, and its corresponding real contact area was also small, resulting in a decrease in the calculated normal contact stiffness of the tooth surface. Moreover, the larger D is, the greater the number of the asperities per unit area is. The increase in G will cause a greater the amplitude of the asperity, a greater the load borne by a single asperity, and a greater influence of the lateral contact and interaction of asperity. Overall, the greater the load, the greater the lateral contact and interaction of asperity. The above studies show that the influence of the lateral contact and interaction of the asperities cannot be ignored in the investigation of the contact between tooth surfaces. The research results offer the theoretical basis for further accurate study of gear contact.

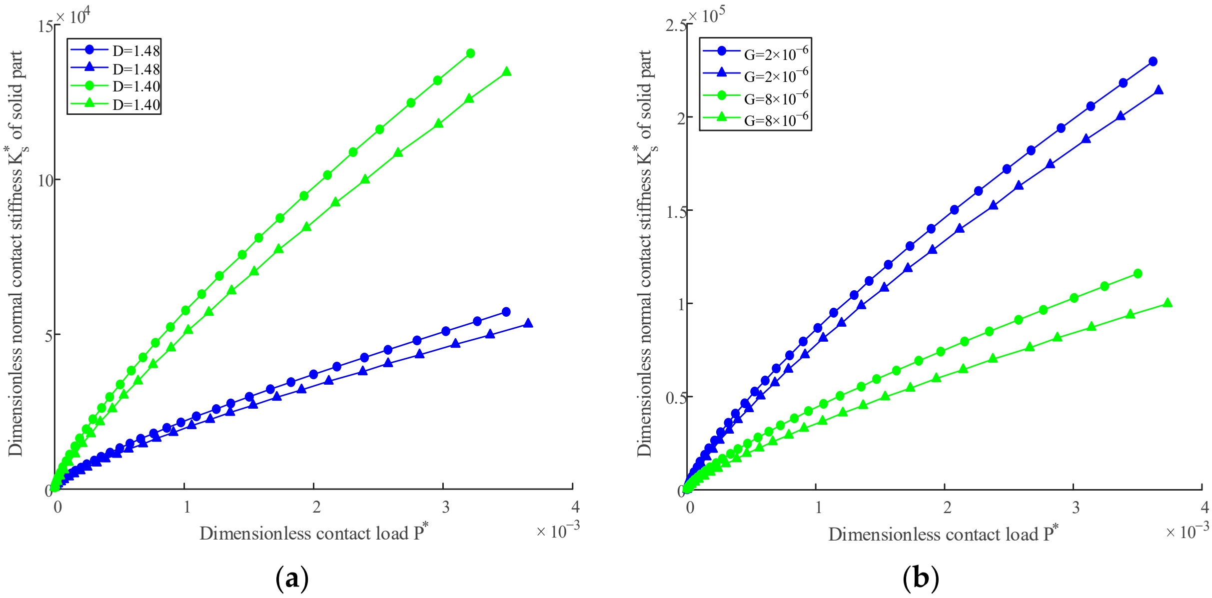

Figure 12. Effect of lateral action of asperity: (**a**) $G = 2 \times 10^{-6}$, (**b**) $D = 1.40$.

5. Conclusions

In this paper, the variation mechanisms of asperity under asperity lateral contact and interaction were considered. Combined with the meshing process of the helical gear pair, the contact surface correction coefficient of helical gear was constructed, and an accurate fractal prediction model of helical gear contact stiffness was derived. Then, the effects of the key factors were further discussed based on the fractal prediction model. Here are some relevant conclusions:

(1) The smaller the correction coefficient of the helical gear contact surface, the greater the impact on the model. The oil film NCS is dominant under a low gear contact load. With an increase in gear contact load, the proportion of oil film NCS decreases rapidly, and, finally, the solid NCS is dominant. The surface topography of the contact material has the greatest effect on the NCS, followed by that of the liquid lubricating medium.

(2) Considering the asperity lateral contact and interaction, the theoretical NCS value calculated under the same conditions is lower. When the load is greater, the lateral effect of asperity is larger and the theoretical value of NCS calculated by this model is more consistent with the actual situation. When D decreases and G increases, the influence of the lateral effect of asperity increases.

(3) By comparing these research results with those of our peers, the model considering asperity lateral contact and interaction in this paper is relatively closer to the experimental data. With the presented achievements, the revised model proposed in this work provides a theoretical foundation for further research on the gear contact surface characteristics.

The research on gear contact in this paper was conducted under a single compression. In fact, the tooth surface will be repeatedly squeezed during the gear-meshing process. In this process, the asperities of the tooth surface will be plastically deformed due to the force, which will affect the subsequent contact characteristics. Therefore, in the follow-up study, the fractal contact characteristics of gears under repeated loading can be considered.

Author Contributions: Conceptualization, X.X. and L.S.; methodology, L.S.; software, L.F.; validation, X.X., L.S. and L.F.; formal analysis, X.X.; investigation, L.S.; data curation, L.F.; writing—original draft preparation, L.S.; writing—review and editing, X.X.; visualization, L.F.; supervision, L.S.; project administration, X.X.; funding acquisition, X.X. All authors have read and agreed to the published version of the manuscript.

Funding: This work was supported by the Foundation of National Key Research and Development Plan of China [No. 2018YFB2001300]; the Foundation of National Natural Science of China [No. 51975078] and [No. 52375042]; the Chongqing Science Fund for Distinguished Young Scholars [cstc2021jcyj-jqX0010]; the Foundation of Chongqing Talent Plan [cstc2022ycjh-bgzxm0130].

Data Availability Statement: The datasets generated during the current study are available from the corresponding author on reasonable request.

Conflicts of Interest: The authors declare no conflict of interest.

Nomenclature

A_0	Nominal contact area
A_{aie}	The elastic contact area
A_{aiep1}	The first stage of elastic–plastic contact area
A_{aiep2}	The second stage of elastic–plastic contact area
A_{aip}	The full plastic contact area
A_e	Elastic contact area
A_{ep1}	The first-stage elastic–plastic contact area
A_{ep2}	The second stage elastic–plastic contact area
A_i	Sum of asperity contact area (when contact angle of the asperity is α_i)
A_j	Long axis of jth ellipsoid
A_p	Plastic contact area
A_r	The total real contact area of the contact surface
a_p	The contact area of asperity positive contact
a_a	The contact area of asperity lateral contact
a_1	Long axis of the contact ellipse
a_{ae}	The contact area in the elastic deformation stage of asperity
a_{aec}	The critical elastic deformation area of asperity
a_{aepc}	The elastic–plastic critical contact area
a_{apc}	The plastic critical contact area
a_c	Critical contact area
a_e	Contact area of a single asperity during elastic deformation stage
a_l	Maximum contact area of a single asperity
b	Short axis of the contact ellipse
D	Fractal dimension
d	The distance between the rigid smooth surface and the average of the original roughness
$d_{1,2}$	The diameter of the gear pitch circle
d_n	The distance between the rigid smooth surface and the average plane of asperity after the normal load deformation of the joint surface
E	The composite Young's modulus of the contact material
F	The unit line load
F_{ae}	The contact load of a single asperity
F_{aep1}	The contact load of a single asperity at the first stage elastic–plastic deformation
F_{aep2}	The contact load of a single asperity at the second stage elastic–plastic deformation
F_{ap}	The contact load of a single asperity in complete plastic stage
G	Roughness amplitude
H	Material hardness
K	The correlation coefficient between hardness H and yield strength Y
K_l	Contact stiffness of oil film part
K_n	Normal contact stiffness
K_s	The NCS of Solid Part
k_{sae}	The NCS of a single asperity in elastic stage
k_{sae1}	The NCS of a single asperity in the first stage of elastic–plastic
k_{saep2}	The NCS of a single asperity in the second elastic–plastic stage
$k_{S\alpha_i}$	The NCS when the contact angle is α_i
k_μ	The friction correction coefficient

a_p	Contact area of a single asperity during plastic deformation stage	n	The frequency index of asperity
B_j	Short axis of j th ellipsoid	$n(a)$	Island area distribution function
$n(a)'$	Gear asperity distribution function	Y	The yield strength of softer materials
P_{aie}	The elastic contact load	y	The offset between the intersection midpoint of the asperity and the peak value of the rough surface
P_{aiep1}	The first stage of the elastic–plastic contact load	$z(x)$	The random height of the rough surface profile
P_{aiep2}	The second stage elastic–plastic contact load	α	Contact angle of the asperity
P_{aip}	The full plastic contact load	α_t	The pressure angle of the end face
p	Subscript to indicate the plastic deformation stage	α_t'	The meshing angle
p_m	The average contact pressure.	β_b	The spiral angle of the base circle
$P_n(x,y)$	the total normal force at the contact surface (x, y)	δ_1	The total deformation considering asperity interaction
P_μ	The critical average pressure	δ_a	The contact deformation in a direction considering asperity lateral contact and interaction
P_1	The force exerted on the rough peak	δ_{aec}	The elastic critical deformation of asperity
R	Radius of curvature at the vertex of the asperity	δ_p	The asperity positive contact deformation
$R_{1,2}$	The node normal curvature radius of driving gear and driven gear	δ'	The displacement of the mean plane caused by the interaction between asperities
$R(y)$	The equivalent curvature radius of the contact points of the two asperities	λ_C	Correction coefficient of contact surface
R_s	Sum of two asperity radii	ρ	Comprehensive radius of curvature of the contact body
r_a	Tangential offset of the contact asperities	γ^n	The spatial frequency of the rough surface profile
S	Gear contact area	$\Delta P_{\mathrm{ae}}(a)$	The contact stress of asperity in elastic deformation stage
X_h	Gear comprehensive curvature coefficient		

References

1. Machado, M.; Moreira, P.; Flores, P.; Lankarani, H.M. Compliant contact force models in multibody dynamics: Evolution of the Hertz contact theory. *Mech. Mach. Theory* **2012**, *53*, 99–121. [CrossRef]
2. Greenwood, J.A.; Williamson, J.B.P. Contact of nominally flat surfaces. *Proc. R. Soc. Lond. Ser. A Math. Phys. Sci.* **1966**, *295*, 300–319.
3. Kogut, L.; Etsion, I. Elastic-plastic contact analysis of a sphere and a rigid flat. *J. Appl. Mech.* **2002**, *69*, 657–662. [CrossRef]
4. Majumdar, A.; Bhushan, B. Fractal Model of Elastic-Plastic Contact between Rough Surfaces. *ASME J. Tribol.* **1991**, *113*, 1–11. [CrossRef]
5. Liu, P.; Zhao, H.; Huang, K.; Chen, Q.; Xiong, Y. Study on improved fractal model of normal contact stiffness of line segment gear. *Chin. J. Mech. Eng.* **2018**, *54*, 114–122. [CrossRef]
6. Huang, K.; Xiong, Y.; Wang, T.; Chen, Q. Research on the dynamic response of high-contact-ratio spur gears influenced by surface roughness under EHL condition. *Appl. Surf. Sci.* **2017**, *392*, 8–18. [CrossRef]
7. Wang, H.; Jia, P.; Wang, L.; Yun, F.; Wang, G.; Liu, M.; Wang, X. Modeling of the loading–unloading contact of two cylindrical rough surfaces with friction. *Appl. Sci.* **2020**, *10*, 742. [CrossRef]
8. Wang, X.; Liu, S. Fractal estimation model of normal contact stiffness of micro-pitting gear. *Chin. J. Mech. Eng.* **2021**, *57*, 68–76.
9. Wang, R.; Zhu, L.; Zhu, C. Research on fractal model of normal contact stiffness for mechanical joint considering asperity interaction. *Int. J. Mech. Sci.* **2017**, *134*, 357–369. [CrossRef]
10. Zhou, C.; Huang, F.; Han, X.; Gu, Y. An elastic–plastic asperity contact model and its application for micro-contact analysis of gear tooth profiles. *Int. J. Mech. Mater. Des.* **2017**, *13*, 335–345. [CrossRef]
11. Chen, D.; Hou, L.; Guo, T. Simulation method of elastic asperity body hierarchical contact based on fractal geometric reconstruction and lateral contact mechanics model. *Chin. J. Mech. Eng.* **2018**, *54*, 117–124. [CrossRef]
12. Zhang, K.; Li, G.; Gong, J.; Zhang, M. Normal contact stiffness of rough surfaces considering oblique asperity contact. *Adv. Mech. Eng.* **2019**, *11*, 1–14. [CrossRef]
13. Liu, P.; Zhao, H.; Huang, K.; Chen, Q. Research on normal contact stiffness of rough surface considering friction based on fractal theory. *Appl. Surf. Sci.* **2015**, *349*, 43–48. [CrossRef]
14. Berry, M.V.; Lewis, Z.V.; Nye, J.F. On the Weierstrass-Mandelbrot fractal function. *Proc. R. Soc. Lond. A Math. Phys. Sci.* **1980**, *370*, 459–484.
15. Li, X.; Li, Z.; Jin, S.; Zhang, J. A multi-scale model of real contact area for linear guideway based on the fractal theory. *Proc. Inst. Mech. Eng. Part C J. Mech. Eng. Sci.* **2021**, *235*, 5796–5813. [CrossRef]
16. Sepehri, A.; Farhang, K. On elastic interaction of nominally flat rough surfaces. *J. Tribol.* **2008**, *130*, 011014. [CrossRef]
17. Li, L.; Wang, J.; Shi, X.; Ma, S.; Cai, A. Contact stiffness model of joint surface considering continuous smooth characteristics and asperity interaction. *Tribol. Lett.* **2021**, *69*, 43. [CrossRef]

18. Ciavarella, M.; Greenwood, J.A.; Paggi, M. Inclusion of "interaction" in the Greenwood and Williamson contact theory. *Wear* **2008**, *265*, 729–734. [CrossRef]
19. Briscoe, B.J. Contact mechanics. *Tribol. Int.* **1986**, *19*, 109–110. [CrossRef]
20. Tang, D.; Xiang, G.; Guo, J.; Cai, J.; Yang, T.; Wang, J.; Han, Y. On the optimal design of staved water-lubricated bearings driven by tribo-dynamic mechanism. *Phys. Fluids* **2023**, *35*, 093611. [CrossRef]
21. Marjanovic, N.; Ivkovic, B.; Blagojevic, M.; Stojanovic, B. Experimental determination of friction coefficient at gear drives. *J. Balk. Tribol. Assoc.* **2010**, *16*, 517–526.
22. Wang, Y.; Zhang, X.; Wen, S.; Chen, Y. Fractal loading model of the joint interface considering strain hardening of materials. *Adv. Mater. Sci. Eng.* **2019**, *2019*, 2108162. [CrossRef]
23. Xiao, H.; Sun, Y.; Chen, Z. Fractal modeling of normal contact stiffness for rough surface contact considering the elastic–plastic deformation. *J. Braz. Soc. Mech. Sci. Eng.* **2019**, *41*, 11. [CrossRef]
24. Ma, D.; Hou, L.; Wei, X.; Chen, J. Simple Mechanical Model of Sliding Friction Contact of Circular Arc Gear Based on Fractal Theory. *Chin. J. Mech. Eng.* **2016**, *52*, 121–127. [CrossRef]
25. Zhou, C.; Wang, H. An adhesive wear prediction method for double helical gears based on enhanced coordinate transformation and generalized sliding distance model. *Mech. Mach. Theory* **2018**, *128*, 58–83. [CrossRef]
26. Xue, P.; Zhu, C.; Wang, R.; Zhu, L. Research on dynamic characteristics of oil-bearing joint surface in slide guides. *Mech. Based Des. Struct. Mach.* **2022**, *50*, 1893–1913. [CrossRef]
27. Xiao, Z.; Shi, X.; Wang, X.; Ma, X.; Han, Y. Lubrication analysis and wear mechanism of heavily loaded herringbone gears with profile modifications in full film and mixed lubrication point contacts. *Wear* **2021**, *477*, 203790. [CrossRef]